OPEN

Citation: Cell Death and Disease (2014) 5, e1188; doi:10.1038/cddis.2014.129

www.nature.com/cddis

Reduced IRE1α mediates apoptotic cell death by disrupting calcium homeostasis via the InsP3 receptor

SM Son[1], J Byun[1], S-E Roh[2], SJ Kim[2] and I Mook-Jung*[,1]

The endoplasmic reticulum (ER) is not only a home for folding and posttranslational modifications of secretory proteins but also a reservoir for intracellular Ca^{2+}. Perturbation of ER homeostasis contributes to the pathogenesis of various neurodegenerative diseases, such as Alzheimer's and Parkinson diseases. One key regulator that underlies cell survival and Ca^{2+} homeostasis during ER stress responses is inositol-requiring enzyme 1α (IRE1α). Despite extensive studies on this ER membrane-associated protein, little is known about the molecular mechanisms by which excessive ER stress triggers cell death and Ca^{2+} dysregulation via the IRE1α-dependent signaling pathway. In this study, we show that inactivation of IRE1α by RNA interference increases cytosolic Ca^{2+} concentration in SH-SY5Y cells, leading to cell death. This dysregulation is caused by an accelerated ER-to-cytosolic efflux of Ca^{2+} through the InsP3 receptor (InsP3R). The Ca^{2+} efflux in IRE1α-deficient cells correlates with dissociation of the Ca^{2+}-binding InsP3R inhibitor CIB1 and increased complex formation of CIB1 with the pro-apoptotic kinase ASK1, which otherwise remains inactivated in the IRE1α–TRAF2–ASK1 complex. The increased cytosolic concentration of Ca^{2+} induces mitochondrial production of reactive oxygen species (ROS), in particular superoxide, resulting in severe mitochondrial abnormalities, such as fragmentation and depolarization of membrane potential. These Ca^{2+} dysregulation-induced mitochondrial abnormalities and cell death in IRE1α-deficient cells can be blocked by depleting ROS or inhibiting Ca^{2+} influx into the mitochondria. These results demonstrate the importance of IRE1α in Ca^{2+} homeostasis and cell survival during ER stress and reveal a previously unknown Ca^{2+}-mediated cell death signaling between the IRE1α–InsP3R pathway in the ER and the redox-dependent apoptotic pathway in the mitochondrion.

Cell Death and Disease (2014) **5,** e1188; doi:10.1038/cddis.2014.129; published online 17 April 2014
Subject Category: Neuroscience

The endoplasmic reticulum (ER) is an intracellular organelle not only responsible for protein synthesis and quality control but also serves as a Ca^{2+} store to maintain intracellular Ca^{2+} levels.[1,2] Most integral membrane proteins and secretory proteins are synthesized at the ER, where they fold and, when necessary, become covalently modified and assembled into high-quality, functional proteins. As the maintenance of ER homeostasis is essential to cell survival, the cells have an ER stress-sensing system, termed the 'unfolded protein response' (UPR).[3,4] The ER dysfunctions such as glucose deprivation, aberrant Ca^{2+} regulation, or accumulation of misfolded proteins, leads to UPR activation and initiates intracellular signaling pathways for cell protection. The UPR is governed by ER stress sensors, including inositol-requiring enzyme 1α (IRE1α), double-stranded RNA-activated protein kinase (PKR)-like ER kinase (PERK), and activating transcription factor 6 (ATF6), in the ER lumen.[5] IRE1α, a major ER stress transducer, is a serine/threonine protein kinase/endoribonuclease that, upon activation, initiates the splicing of X-box binding protein 1 (Xbp-1) mRNA.[6,7] Spliced Xbp-1 mRNA encodes a transcriptional activator that induces the transcription of chaperone protein-encoding genes, whose products have a role in ER protein folding.[7] Under prolonged stress, IRE1α also interacts with TNF receptor-associated factor 2 (TRAF2) and apoptosis signal-regulating kinase 1 (ASK1) or activates caspase-12, an ER resident caspase, to cause cell death in neuronal cells.[8,9] PERK is a transmembrane kinase that phosphorylates eukaryotic translation initiation factor 2 subunit alpha (eIF2α), thereby reducing protein synthesis and counteracting ER protein overload.[10] eIF2α phosphorylation also allows selective translation of certain mRNA molecules that contain small open reading frames in their 5′ untranslated regions, which in turn leads to the production of transcriptional activators, such as ATF4.[11] ATF6 is a membrane-bound transcription factor that drives transcription in the ER stress response. In response to protein

[1]Department of Biochemistry and Biomedical Sciences, Seoul National University College of Medicine, Seoul, Korea and [2]Department of Physiology, Seoul National University College of Medicine, Seoul, Korea
*Corresponding author: I Mook-Jung, Department of Biochemistry and Biomedical Sciences, Seoul National University College of Medicine, 28 Yungun-dong, Jongro-gu, Seoul 110-799, Korea. Tel: +82 2 740 8245; Fax: +82 2 3672 7352; E-mail: inhee@snu.ac.kr
Keywords: Ca^{2+}; cell death; InsP3R; IRE1α; mitochondrial dysfunction
Abbreviations: ER, endoplasmic reticulum; ASK1, apoptosis signal-regulating kinase 1; IRE1α, inositol-requiring enzyme 1α; InsP3R, inositol-1,4,5-triphosphate (InsP3) receptor; CIB1, calcium- and integrin-binding protein 1; ROS, reactive oxygen species; UPR, unfolded protein response; PERK, double-stranded RNA-activated protein kinase (PKR)-like ER kinase; ATF6, activating transcription factor 6; TRAF2, TNF receptor-associated factor 2; eIF2α, eukaryotic translation initiation factor 2 subunit alpha; RyR, ryanodine receptor; SERCA, Ca^{2+} reuptake pumps consisting of sarco-endoplasmic reticulum Ca^{2+}-ATPase; TUNEL, terminal deoxynucleotidyl transferase dUTP nick end labeling; TUDCA, tauroursodeoxycholate; TMRM, tetramethyl rhodamine methyl ester; MCU, mitochondrial uniporter; CsA, cyclosporin A; Fura-2 AM, fura-2 acetoxymethyl ester; Xbp-1, X-box binding protein 1
Received 16.10.13; revised 28.1.14; accepted 27.2.14; Edited by D Bano

misfolding, the ATF6 cytoplasmic domain is liberated from its membrane anchor by regulated proteolysis.[12]

The intracellular Ca^{2+} ion level ($[Ca^{2+}]_i$) regulates cellular processes, such as exocytosis, transcription, proliferation, and apoptosis.[13] The Ca^{2+} concentration is tightly regulated by multiple Ca^{2+} channels, pumps, and binding proteins; $[Ca^{2+}]_i$ is increased by Ca^{2+} influx across the plasma membrane and Ca^{2+} release from intracellular stores. The ER, mitochondria, and nucleus are main intracellular Ca^{2+} stores; the ER is the most important, as it can store up to 10–100 mM Ca^{2+} (*versus* 100–300 nM in the cytoplasm).[14] Ca^{2+} movements across the ER membrane are facilitated by Ca^{2+} release channels, including inositol-1,4,5-triphosphate (InsP3) receptors (InsP3Rs) and ryanodine receptors (RyRs); and Ca^{2+} reuptake pumps consisting of sarco-endoplasmic reticulum Ca^{2+}-ATPases (SERCAs) residing in the ER.[15–17] The pumps, channels, and buffering proteins finely regulate the spatiotemporal pattern of cytosolic Ca^{2+} levels ($[Ca^{2+}]_{cytosol\ (c)}$). However, despite tight regulation of Ca^{2+} release from the ER, the depletion of ER Ca^{2+} and the overload of cytosolic Ca^{2+} can be induced by several stimuli. The alterations in $[Ca^{2+}]_c$ disrupt Ca^{2+} homeostasis, and unchecked increases in $[Ca^{2+}]_c$ can trigger apoptosis through the activation of processes in the cytoplasm (e.g., abnormal activation of calpain or phosphatase calcineurin), activation of ER resident caspases, or mitochondrial dysfunction due to Ca^{2+} overload.[18–20]

As ER stress is intimately associated with cell death, proper manipulation of ER stress is essential for cell survival.[21] In this study, we investigated the role of ER stress transducers in cell death. By using IRE1α-, PERK-, or ATF6-specific siRNA, we demonstrated that knockdown (KD) of IRE1α, but not PERK or ATF6, induced ER stress and altered morphology (ER expansion). In SH-SY5Y cells, IRE1α KD caused cell death, not due to unfolded protein accumulation but due to accelerated Ca^{2+} release from the ER. In addition, IRE1α-KD-induced $[Ca^{2+}]_i$ alterations were mediated by InsP3R. We speculate that IRE1α may regulate InsP3R-mediated Ca^{2+} release by interacting with ASK1 and calcium- and integrin-binding protein 1 (CIB1), the latter of which regulates opening of InsP3R.[22] In IRE1α-KD cells, InsP3R-induced increases of ER Ca^{2+} release resulted in cell death due to prolonged mitochondrial Ca^{2+} accumulation and alterations in morphology (swelling and fragmentation) and function.

Results

Reduced IRE1α levels induce ER stress and alter ER morphology in human neuroblastoma SH-SY5Y cells. Previous studies have shown that ER stress causes cell death through accumulation of unfolded or abnormal proteins in the ER and subsequent activation of ER stress-induced caspases.[20,23] ER stress transducers modulate ER-specific stress;[7,10,24] therefore, we investigated whether the main ER stress transducer IRE1α regulates ER stress-mediated cell death. After SH-SY5Y cells were transfected with IRE1α-specific siRNA for 48 h, total IRE1α levels were reduced by 40–60% *versus* control siRNA-transfected cells, without changes in β-actin expression (Figures 1a–c and Supplementary Figures S1a and b). We used western blots to determine whether downregulation of IRE1α expression induces ER stress and observed marked induction of CHOP, an ER stress-related marker protein, as well as GRP78, an ER chaperone[25] (Figure 1b). Next, we knocked down other ER stress transducers, PERK and ATF6α, to test their ability to regulate ER stress. PERK- and ATF6α-specific siRNA reduced their respective protein levels by 60–80%, without any change in β-actin expression (Figure 1a). We found, however, unlike IRE1α KD, reduction of PERK or ATF6α did not induce ER stress (Figure 1c), suggesting that only IRE1α regulates ER stress under basal conditions. As IRE1α is localized in the ER membrane[26] and the ER structure undergoes dramatic changes upon cellular damage,[27,28] we examined ER morphology under IRE1α KD. Western blotting revealed no difference in the expression of ER membrane proteins, such as calreticulin or calnexin (Figure 1d). Immunofluorescence experiments using anti-calreticulin antibody as an ER indicator showed that ER morphology was slightly altered in IRE1α-KD cells (data not shown). We used transmission electron microscopy to analyze IRE1α-KD-induced changes in ER morphology. The electron micrographs of IRE1α-KD cells showed ER enlargement and distension (ER expansion) (Figure 1e). Thus, IRE1α KD induced ER stress and caused ER expansion.

Knockdown of IRE1α induces cell death by disrupting intracellular Ca^{2+} homeostasis. ER stress induces cell death;[21] therefore, we tested the effect of IRE1α KD on cell viability. The results of MTT and calcein-AM assays showed that reduction of IRE1α induced cell death (Figures 2a and b). To confirm the increase of apoptotic cell death under IRE1α-KD conditions, we performed the terminal deoxynucleotidyl transferase dUTP nick end labeling (TUNEL) assay, a method for detecting DNA fragmentation. Consistently, TUNEL staining indicated increased apoptosis in IRE1α-KD cells (Figure 2c). To determine whether this cell death was mediated by ER stress, the IRE1α-KD cells were treated with the chemical chaperone tauroursodeoxycholate (TUDCA)[29] to protect the cells from ER stress. Indeed, TUDCA alleviated ER stress induction by IRE1α-KD (Figure 2e) but did not rescue IRE1α-KD-induced cell death (Figure 2d), suggesting that IRE1α-KD-induced cell death could not be rescued by inhibiting ER stress alone. Tunicamycin, an inhibitor of protein glycosylation, causes ER stress-induced apoptosis by accumulating unfolded or misfolded proteins in the ER.[30] In this study, tunicamycin not only induced cell death in the SH-SY5Y cells but also enhanced cell death in IRE1α-KD *versus* control siRNA-transfected cells (Figure 2d). These data suggest that IRE1α-KD-induced cell death is mediated by mechanisms other than ER stress caused by accumulation of abnormal proteins in the ER. Previous studies have shown that dysregulation of intracellular Ca^{2+} levels ($[Ca^{2+}]_i$) induces cell death.[13] As IRE1α is a type I transmembrane protein localized in the Ca^{2+}-storing ER,[6] we examined the effect of reduced IRE1α levels on intracellular Ca^{2+} levels. Using the Fluo-4 calcium assay, we observed that IRE1α reduction triggered $[Ca^{2+}]_i$ upregulation (Figure 2f). To determine whether dysregulated $[Ca^{2+}]_i$ induced by IRE1α KD causes cell death, the cells were treated with 1,2-bis(o-aminophenoxy)ethane-*N*,*N*,*N*′,*N*′-tetraacetic

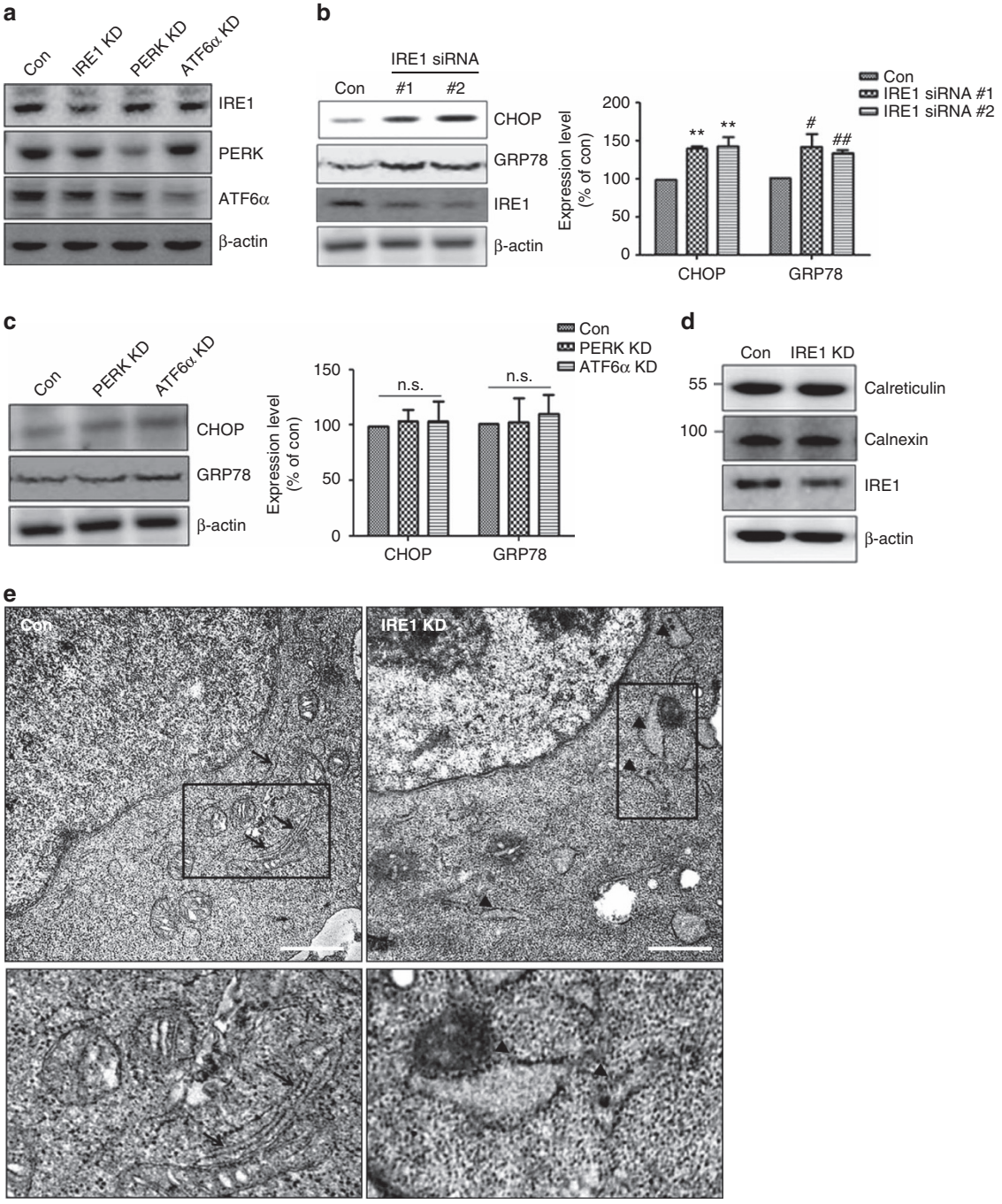

Figure 1 Reduced IRE1α expression induces ER stress and alters ER morphology in human neuroblastoma SH-SY5Y cells. (**a**) Reduced IRE1α, PERK, and ATF6α expression by after siRNA transfection were detected by western blotting. Con indicates control siRNA-transfected cells, and β-actin served as a loading control. (**b**) Induction of ER stress in IRE1α siRNA-transfected cells was examined by western blotting. The IRE1α siRNAs no.1 and no.2 are different siRNA purchased from different companies (no.1 from Santa Cruz and no.2 from Bioneer). CHOP and GRP78 are ER stress marker proteins. Data are shown as the mean percentage ± S.E.M. $^{\#}P<0.05$; **, $^{\#\#}P<0.01$, *versus* control siRNA-transfected cells. Data were obtained from at least three replicates for each group ($N=3$ independent experiments). (**c**) PERK or ATF6α knockdown had no role in ER stress induction. Control, PERK, and ATF6α siRNA were transfected into SH-SY5Y for 48 h. Representative bands are shown. Data are shown as the mean percentage ± S.E.M.; NS indicates no significant difference *versus* control siRNA-transfected cells. $N=4$ experiments. (**d**) Expression of ER-resident proteins (calreticulin and calnexin) was not altered after transfection with IRE1α siRNA. Representative bands are shown. (**e**) EM analysis revealed changes in ER morphology in IRE1α-KD cells. The arrows in control siRNA-transfected cells show normal ER morphology, and the arrowheads in IRE1α-KD cells indicate expanded ER. Scale bars represent 2 μm

acid-acetoxymethyl ester (BAPTA-AM), a Ca^{2+} chelator. BAPTA-AM treatment prevented IRE1α-KD-induced cell death (Figure 2g), suggesting that dysregulation of $[Ca^{2+}]_i$ has a role in IRE1α-KD-induced cell death. Neither PERK nor ATF6α induced ER stress (Figure 1c); we explored their role in cell death by MTT and calcein-AM assays and found that knockdown of these regulators did not induce apoptosis (Figures 2h and i). Consistently, reduction of PERK or ATF6α

had no effect on $[Ca^{2+}]_i$ (Figure 2j). These results suggest that only IRE1α regulates cell survival by maintaining Ca^{2+} homeostasis under basal conditions.

Rescue of IRE1α restores disrupted intracellular Ca^{2+} homeostasis and then inhibits cell death in IRE1α-KD cells. To avoid off-target effects during siRNA treatment, we reintroduced IRE1α into IRE1α-KD cells. After transfection with control or IRE1α siRNA for 24 h, an exogenous IRE1α construct was transfected into the cells for 24 h (Supplementary Figure S2). IRE1α expression was increased in these IRE1α-overexpressing (IRE1 o/e) cells (Supplementary Figure S2a). IRE1α re-introduction rescued calcein-AM signal loss in IRE1α-KD cells (Supplementary Figure S2b), indicating that altered IRE1α levels regulated cell death. Figures 2e and f show that IRE1α regulated cell survival by maintaining Ca^{2+} homeostasis under basal conditions. IRE1α re-introduction also restored $[Ca^{2+}]_i$ in

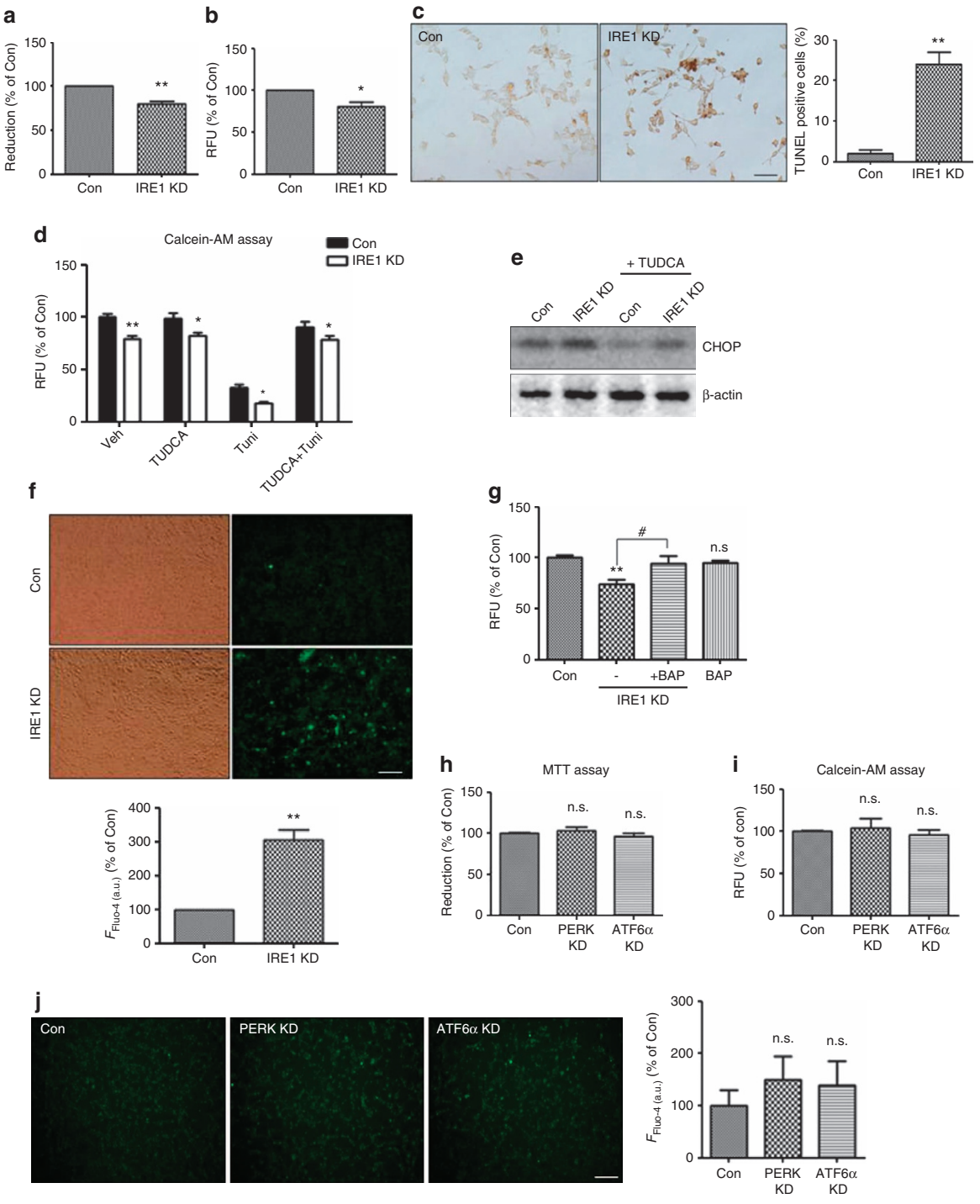

IRE1α-KD cells, as demonstrated by Fluo-4 calcium assay (Supplementary Figure S2c). These data indicate that IRE1α regulates cell survival by maintaining Ca^{2+} homeostasis under basal conditions.

IRE1α KD induces $[Ca^{2+}]_i$ upregulation by accelerating ER Ca^{2+} release. As IRE1α is an ER membrane protein[6] and the ER is a major Ca^{2+}-storing organelle,[1] we investigated whether IRE1α-KD-induced $[Ca^{2+}]_i$ increases are caused by ER Ca^{2+} release. Thapsigargin, an inhibitor of ER Ca^{2+}-ATPase (SERCA),[31] was used to determine the concentration of free Ca^{2+} within the ER lumen ($[Ca^{2+}]_{ER}$) by selectively depleting ER Ca^{2+} stores, whereas BAPTA-AM was used to deplete cytoplasmic Ca^{2+}. The Fluo-4 assay showed that the IRE1α-KD cells showed few Ca^{2+} level released from ER, compared with control siRNA-transfected cells (Figure 3a), suggesting that increased $[Ca^{2+}]_i$ in the IRE1α-KD cells was caused by ER Ca^{2+} release. To confirm this result, we directly measured the effects of IRE1α downregulation by Ca^{2+} imaging with the fluorescent dye Fura-2-AM. Although the IRE1α-KD cells showed increases in the basal $[Ca^{2+}]_i$, the levels of $[Ca^{2+}]_i$ increases in the IRE1α-KD cells after challenge with thapsigargin (a measure of $[Ca^{2+}]_{ER}$ stores) was lower than that in the control siRNA-transfected cells (Figure 3b). The experiment was repeated three times; the average increase after thapsigargin challenge was 48% of the control level (average baseline level). These data indicate that reduced IRE1α levels caused $[Ca^{2+}]_i$ upregulation by accelerating Ca^{2+} release from the ER.

InsP3R mediates IRE1α-KD-induced $[Ca^{2+}]_i$ alterations and increases ER Ca^{2+} release resulting in cell death. The ER is the most important intracellular Ca^{2+} store.[32] Regulation of intracellular Ca^{2+} by the ER is mainly mediated by Ca^{2+} uptake into the ER through SERCA Ca^{2+} pumps and Ca^{2+} release through Ca^{2+} channels, such as InsP3Rs or RyRs.[33–35] To determine whether $[Ca^{2+}]_i$ increases in IRE1α-KD cells are caused by ER Ca^{2+}-related channels, we treated the cells with Ca^{2+} channel blockers dantrolene and 2-aminoethoxydiphenyl borate (2-APB) to inhibit RyRs and InsP3R, respectively. As shown in Figure 4a, 2-APB treatment blocked the increase of $[Ca^{2+}]_i$ in the IRE1α-KD cells, whereas dantrolene did not. Notably, western blotting indicates no difference in RyRs and InsP3R expression between IRE1α-KD and control siRNA-transfected cells (Figure 4b), suggesting that upregulation of $[Ca^{2+}]_i$ in the IRE1α-KD cells is associated with InsP3R but does not alter the expression of ER Ca^{2+}-related channels. Next, to determine whether InsP3R-mediated Ca^{2+} release in IRE1α-KD cells influences cell death, the viability of IRE1α-KD cells treated with vehicle, dantrolene, or 2-APB was determined by calcein-AM assay. Inhibition of InsP3R rescued cell death in the IRE1α-KD cells, whereas the blocker of RyRs (dantrolene) did not (Figure 4c). To confirm this result, caspase-3 and -9 activities were measured. Essential for apoptosis,[36,37] caspases exist as inactive zymogens and require proteolytic processing for activation. Under apoptotic conditions, the activation of upstream caspases (caspase-8 and/or -9) proteolytically activates downstream caspases, such as caspase-3.[38] In comparison to control siRNA-transfected cells, the IRE1α-KD cells showed increased levels of cleaved caspase-3 and -9 (Figure 4d); these effects were rescued by 2-APB, but not dantrolene. To confirm these results, the cells were treated with xestospongin C (XeC), an InsP3R-specific antagonist.[39] XeC reversed $[Ca^{2+}]_i$ increases and IRE1α-KD-induced cell death in the IRE1α-KD cells (Figures 4e and f). These data suggest that, upon IRE1α downregulation, InsP3R-mediated Ca^{2+} release induces apoptotic cell death.

IRE1α regulates InsP3R-mediated Ca^{2+} release through the ASK1-CIB1 interaction. To explore the mechanisms through which IRE1α KD promoted InsP3R-mediated Ca^{2+} release, we tested whether IRE1α interacts directly with InsP3R. By co-immunoprecipitation (co-IP), no interaction was detected between IRE1α and InsP3R (Figure 5a). We next investigated whether IRE1α downstream signaling is associated with InsP3R-mediated Ca^{2+} release in the IRE1α-KD cells. When the IRE1α kinase activity was inhibited by addition of the ATP-competitive inhibitor 1NM-PP1[40] to the SH-SY5Y cells, $[Ca^{2+}]_i$ was not affected (Supplementary Figure S3), suggesting that the IRE1α kinase activity and its downstream signaling pathway are not associated with the opening of InsP3R. Previous studies have demonstrated that CIB1 binding to InsP3R led to an inhibition of Ca^{2+} release from InsP3R.[22] CIB1 was recently suggested to function as a Ca^{2+}-sensitive modulator by interacting directly with ASK1.[41] Based on these findings, we tested the association between the regulation of the opening of InsP3R and

Figure 2 IRE1α KD induces cell death by disrupting intracellular Ca^{2+} homeostasis. (**a**-**c**) After transfection with IRE1α siRNA for 48 h, cell viability was determined by MTT assay (**a**), calcein-AM assay (**b**), and TUNEL assay (**c**). In all, 5×10^3 cells (for MTT and calcein-AM assay) or 1×10^3 cells (for TUNEL assay) were incubated for 24 h after seeding in 96-well plates and were then transfected with control or IRE1α siRNA for 48 h. Data are presented as mean ± S.E.M. $^*P<0.05$; $^{**}P<0.01$ *versus* control siRNA-transfected cells. $N=6$ experiments. Scale bars represent 50 μm. (**d**) An increase in the rate of cell death was observed in IRE1α-KD cells although ER stress was reduced by TUDCA. The control or IRE1α siRNA-transfected cells were incubated with TUDCA (ER chaperone, 100 μM for 12 h) and/or Tuni (Tunicamycin; ER stress inducer; 0.2 μg/μl for 12 h), and then calcein-AM assay was performed to measure the rate of cell death. Data were obtained from at least five replicates for each group ($N=5$ experiments). Values are presented as mean ± S.E.M. $^*P<0.05$; $^{**}P<0.01$ *versus* control siRNA-transfected cells. (**e**) TUDCA reduced ER stress in control and IRE1α-KD cells. CHOP is an ER stress marker protein, and β-actin is a loading control. (**f**) Intracellular Ca^{2+} ($[Ca^{2+}]_i$) was measured by Fluo-4 assay. Cells transfected with control or IRE1α siRNA were incubated for 48 h; 5 μM Fluo-4 AM in DMEM was added at 37 °C for 60 min; fluorescent signals were captured by fluorescence microscopy and analyzed by ImageJ software. Representative images are shown. Scale bars represent 50 μm. $^{**}P<0.01$, when compared with control siRNA-transfected cells. (**g**) The treatment with BAP (BAPTA-AM) rescued IRE1α-KD-induced cell death. After siRNA transfection for 36 h, 5 μM of BAPTA-AM was treated for 12 h, and then calcein-AM assay was performed. $^{**}P<0.01$ (*versus* control siRNA-transfected cells); $^{\#}P<0.05$ (*versus* IRE1α siRNA-transfected cells). NS indicates no significant difference. Data were obtained from at least five replicates per group ($N=5$ experiments). (**h** and **i**) PERK and ATF6α KD cells did not induce cell death in the MTT (**h**) and calcein-AM assay (**i**). Data are the mean percentage ± S.E.M. NS indicates no significant difference. Data were obtained from at least five replicates per group ($N=5$ experiments). (**j**) $[Ca^{2+}]_i$ changes in PERK and ATF6α siRNA KD cells were determined by Fluo-4 assay. Representative images are shown. Scale bars represent 50 μm. Data are the mean percentage ± S.E.M. NS indicates no significant difference

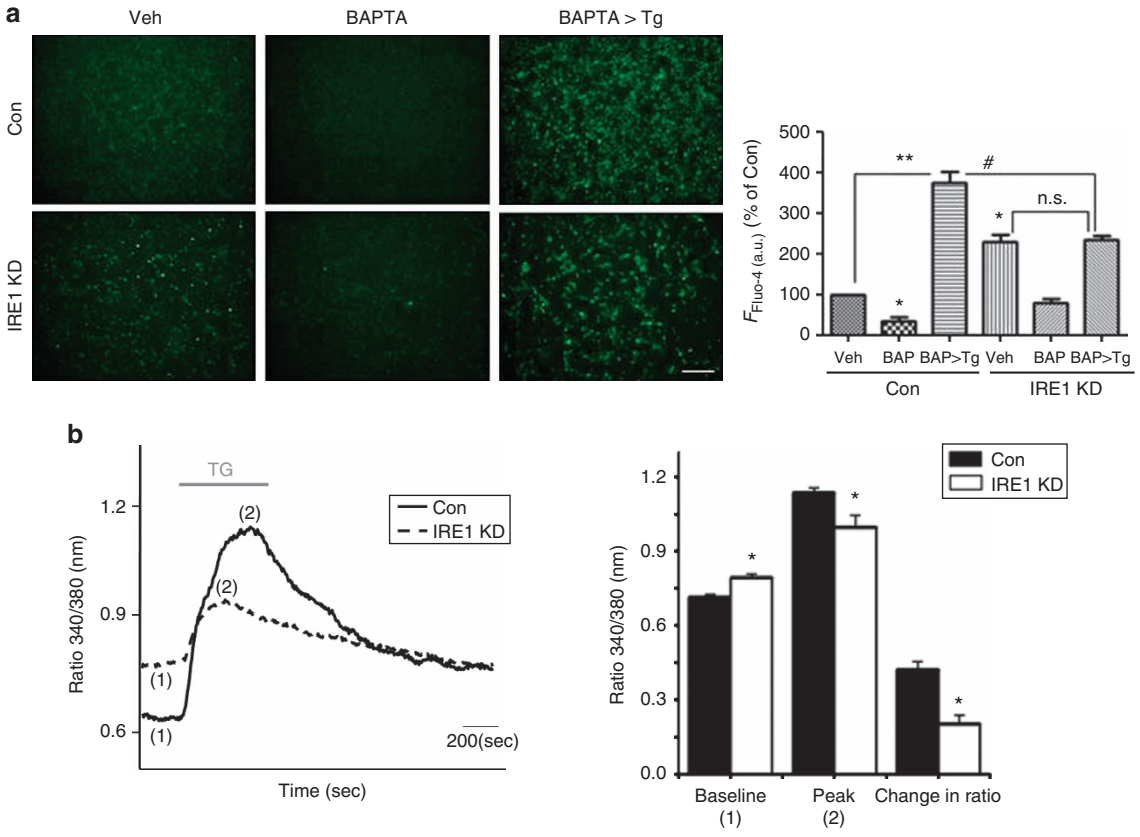

Figure 3 IRE1α KD induces $[Ca^{2+}]_i$ upregulation by accelerating Ca^{2+} release from the ER. (**a**) Changes in $[Ca^{2+}]_i$ were determined by Fluo-4 assay. Thapsigargin (Tg) was used to measure $[Ca^{2+}]_{ER}$. After siRNA-transfection for 48 h, 5 μM Fluo-4-AM in DMEM was added at 37 °C for 60 min. After washing, 5 μM BAPTA-AM was added for 6 h and 0.5 μM thapsigargin for 30 min; fluorescent signals were captured by fluorescence microscopy and analyzed by ImageJ program. Representative images are shown. Scale bars represent 50 μm. Data are shown as the mean percentage ± S.E.M. $^*P<0.05$, $^{**}P<0.01$ (*versus* control siRNA-transfected cells); $^{\#}P<0.05$ (*versus* control siRNA-transfected cells co-treated with BAPTA-AM and thapsigargin). NS indicates no significant difference. (**b**) Ca^{2+} imaging was performed using Fura-2 AM (see also Materials and Methods). The baseline, peak, and change of Fura-2 340 / 380 ratio after thapsigargin were compared between control and IRE1α siRNA-transfected cells. The values represent Fura-2 340 nm/380 nm ratio ± S.E.M. Quantitative data are from at least two independent experiments, where *P*-values are indicated. $^*P<0.05$ *versus* control siRNA-transfected cells

changes in binding partners. The co-IP analysis shows that the extent of the CIB1-ASK1 interaction was increased in the IRE1α-KD cells, compared with the control siRNA-transfected cells. In addition, the IRE1α-KD cells also showed increased CIB1-ASK1 interaction and decreased InsP3R-CIB1 interaction, indicating that IRE1α downregulation reduced recruitment of TRAF2-ASK1 to IRE1α, thereby resulting in increases in free ASK1-CIB1 binding and decreases in the CIB1-InsP3R interaction (Figure 5b). Decreased CIB1-InsP3R interaction induces Ca^{2+} release from InsP3R;[22] thus IRE1α-KD-induced Ca^{2+} release from InsP3R may result from changes in CIB1-InsP3R binding. To visualize the ASK1-CIB1 and CIB1-InsP3R interactions under IRE1α-KD conditions, we performed the proximity ligation assay. In this novel assay, close proximity of the target proteins generates punctate signals. The IRE1α-KD cells produced more signals in the presence of ASK1 and CIB1 antibodies and fewer signals in the presence of CIB1 and InsP3R antibodies (Figure 5c), suggesting that reduced IRE1α levels enhanced ASK1-CIB1 interaction and inhibited CIB1-InsP3R interaction. To determine whether decreased CIB1-InsP3R binding upregulates $[Ca^{2+}]_i$ to trigger cell death, SH-SY5Y cells were transfected with CIB1-specific siRNA (CIB1-KD cells) for 48 h. Reduced CIB1 levels led to $[Ca^{2+}]_i$ increases and cell death; treatment of CIB1-KD cells with 2-APB, but not dantrolene, reversed these effects (Figures 5d and e), suggesting that reduction of CIB1 may upregulate Ca^{2+} release from InsP3R, in turn enhancing cell death.

IRE1α-KD induces mitochondrial dysfunction and reactive oxygen species (ROS) generation, leading to cell death. To investigate the mechanism through which IRE1α-KD-induced $[Ca^{2+}]_i$ increases mediate cell death, we focused on mitochondrial functions because of their role as modulators of the apoptotic process. Previous studies have shown that enhanced $[Ca^{2+}]_i$ mediated by InsP3R and RyRs increased sequestration of vast amounts of Ca^{2+} in mitochondria ($[Ca^{2+}]_{mito}$), which subsequently triggered mitochondrial membrane permeabilization and led to apoptotic cell death.[42] This pathway also depends on Ca^{2+}-induced opening of the permeability transition pore (PTP).[43] As the IRE1α-KD cells showed increased mitochondrial fission (Figure 6a), stable Mito-DsRed-expressing cells were used to investigate the effect of IRE1α KD on mitochondrial morphology. Electron microscopy (EM) showed increased mitochondrial fragmentation in the IRE1α-KD cells (Figure 6b). We also determined the effect of IRE1α KD on

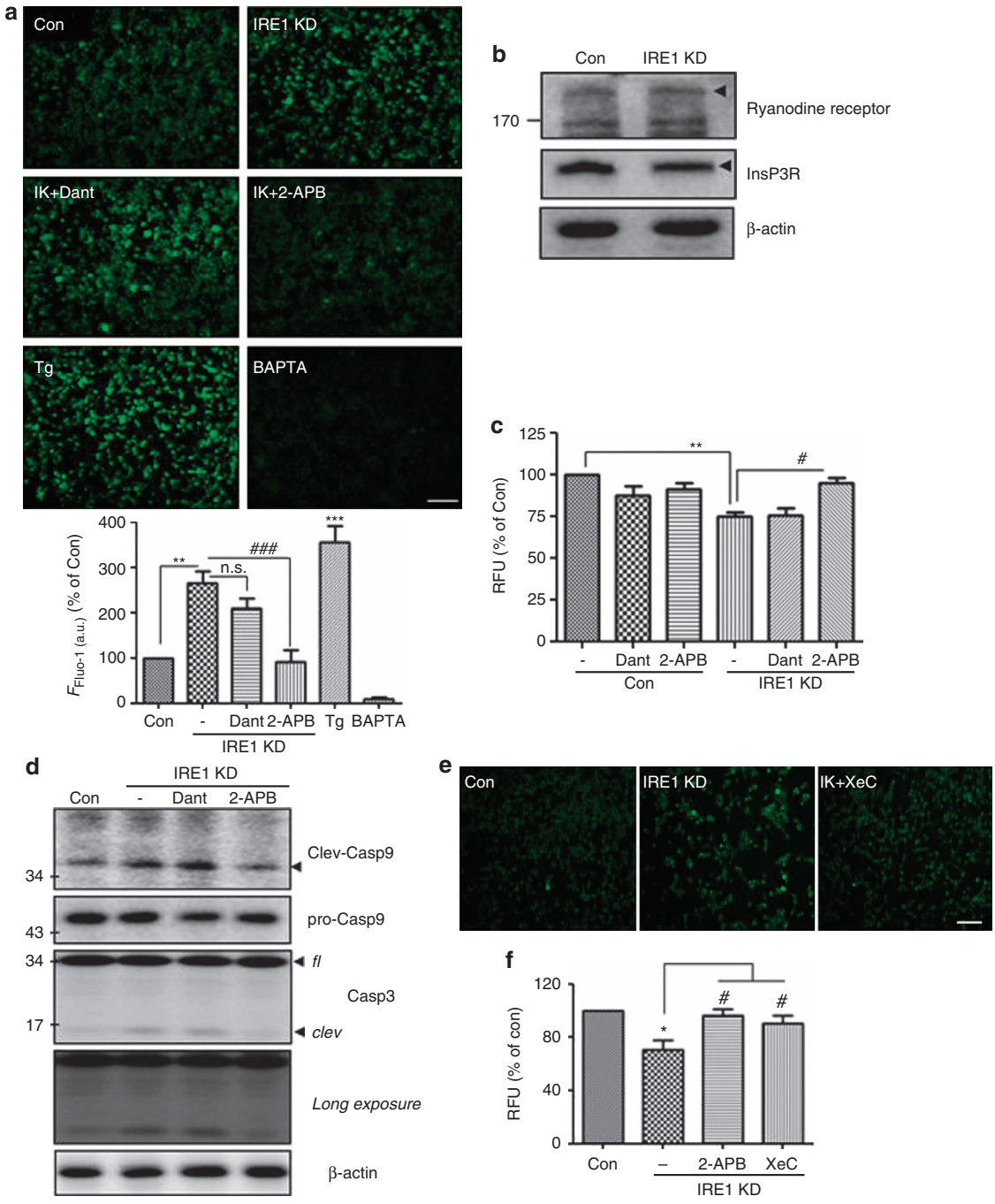

Figure 4 InsP3R mediates IRE1α-KD-induced $[Ca^{2+}]_i$ alterations and increase ER Ca^{2+} release, leading to cell death. (**a**) Treatment with InsP3R blocker (2-APB), not RyRs blocker (Dant; dantrolene), blocked the increase of $[Ca^{2+}]_i$ in the IRE1α-KD cells. Changes in $[Ca^{2+}]_i$ were determined by the Fluo-4 assay. After siRNA transfection for 48 h, 5 μM of Fluo-4 AM in DMEM was added at 37 °C for 60 min. After washing, dantrolene (20 μM), 2-APB (10 μM), and BAPTA-AM (5 μM) were added for 6 h, and 0.5 μM of thapsigargin was treated for 30 min, and then fluorescent signals were captured using a fluorescence microscope and analyzed in ImageJ ($N = 3$ experiments). Data are shown as the mean percentage ± S.E.M. IK, IRE1α-KD cells; Tg, thapsigargin (positive control for Fluo-4 assay); BAPTA, BAPTA-AM (negative control for Fluo-4 assay). $^{**}P < 0.01$ and $^{***}P < 0.001$ *versus* vehicle (DMSO)-treated control siRNA-transfected cells; $^{\#\#\#}P < 0.001$ *versus* vehicle (DMSO)-treated IRE1α-KD cells. NS indicates no significant difference. Scale bar = 40 μm. (**b**) RyRs and InsP3R expression in control and IRE1α siRNA-transfected cells was determined by western blotting, with β-actin as a loading control. (**c**) The viability of the IRE1α-KD cells treated with dantrolene (20 μM), 2-APB (10 μM), and BAPTA-AM (5 μM) was determined by calcein-AM assay. Data shown are the mean percentage ± S.E.M. $^{**}P < 0.01$ *versus* vehicle-treated control siRNA-transfected cells; $^{\#}P < 0.05$ *versus* vehicle-treated IRE1α-KD cells. Data were obtained from at least five replicates per group ($N = 5$ experiments). (**d**) IRE1α-KD cells showed activation of caspase-3 and -9, which was inhibited by 2-APB treatment. fl, full-length form; clev, cleaved (activated) form. β-Actin is a loading control. (**e**) Xestospongin C, one of InsP3R-specific antagonists, reversed increased $[Ca^{2+}]_i$ in IRE1α-KD cells. In all, 2 μM of xestospongin C was treated with Fluo-4 loaded cells for 6 h, and changes in $[Ca^{2+}]_i$ were determined by the Fluo-4 assay. XeC, xestospongin C. Representative images are shown. Scale bar = 40 μm. (**f**) Cell viability was analyzed by calcein-AM assay. 2-APB (10 μM) or xestospongin C (2 μM) were treated with IRE1α-KD cells, and then calcein-AM assay was performed. Data are shown as the mean percentage ± S.E.M. $^{*}P < 0.05$ *versus* vehicle-treated control siRNA-transfected cells; $^{\#}P < 0.05$ *versus* vehicle-treated IRE1α-KD cells. Data were obtained from at least five replicates per group ($N = 5$ experiments)

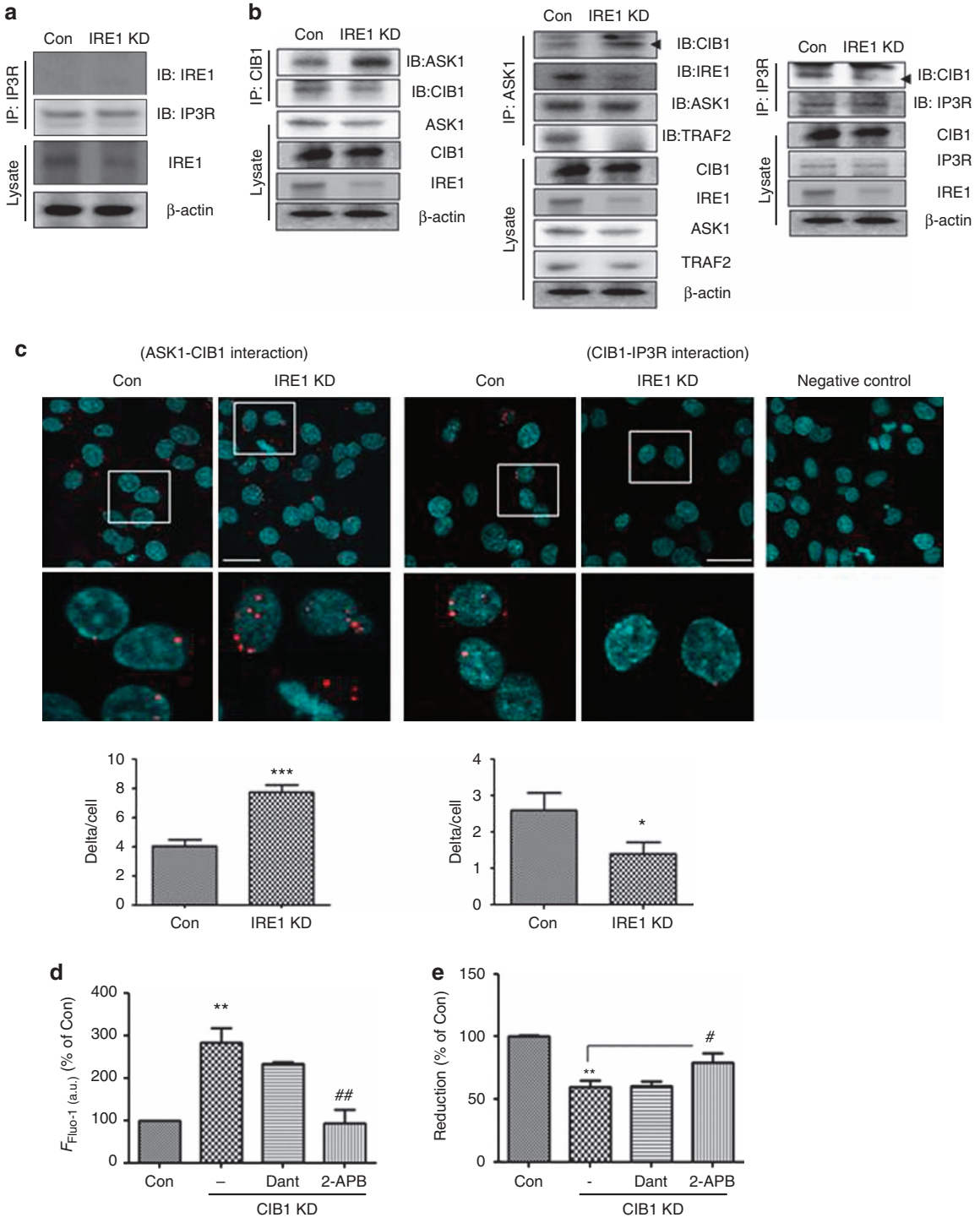

Figure 5 IRE1α regulates InsP3R-mediated Ca^{2+} release through the ASK1-CIB1 interaction. (**a**) Co-immunoprecipitation (IP) with InsP3R- and IRE1α-specific antibodies revealed no interaction between InsP3R and IRE1α. The lower panel ('Lysate') shows a western blot of IRE1α, using the β-actin as a loading marker. Representative images are shown; IP3R indicates InsP3R. (**b**) Co-IP with CIB1-, ASK1-, InsP3R-, and IRE1α-specific antibodies. The left and middle panel show increased CIB1-ASK1 interaction in IRE1α-KD cells. The right panel shows decreased CIB1-InsP3R interaction in IRE1α-KD cells. The lower panel ('Lysate') shows a western blot of ASK1, CIB1, IRE1α, TRAF2, and InsP3R, with β-actin as a loading control. Representative images are shown. (**c**) Proximity ligation assay showed reduced that IRE1α levels induced ASK1-CIB1 interaction and decreased CIB1-InsP3R interaction. DAPI (blue) was used to stain nuclei. Red dot-like signals indicate close proximity of two specific proteins (anti-ASK1 (rabbit polyclonal), anti-CIB1 (mouse monoclonal), and anti-InsP3R (rabbit polyclonal) antibodies). Scale bar = 25 μm. $^{*}P<0.05$ and $^{***}P<0.001$ *versus* control siRNA-transfected cells (Con). (**d**) Alteration in $[Ca^{2+}]_i$ in CIB1-KD cells was measured by Fluo-4 assay. Data were analyzed by ImageJ program. $^{**}P<0.01$ *versus* control siRNA-transfected cells; $^{\#\#}P<0.01$ *versus* CIB1 siRNA-transfected cells. (**e**) Cell viability was analyzed by MTT assay. 2-APB (10 μM) or dantrolene (20 μM) were added to CIB1-KD cells, and the MTT assay was performed. Data shown are the mean percentage ± S.E.M. $^{**}P<0.01$ *versus* control siRNA-transfected cells; $^{\#}P<0.05$ *versus* CIB1-KD cells. Data were obtained from at least five replicates per group ($N=5$ experiments)

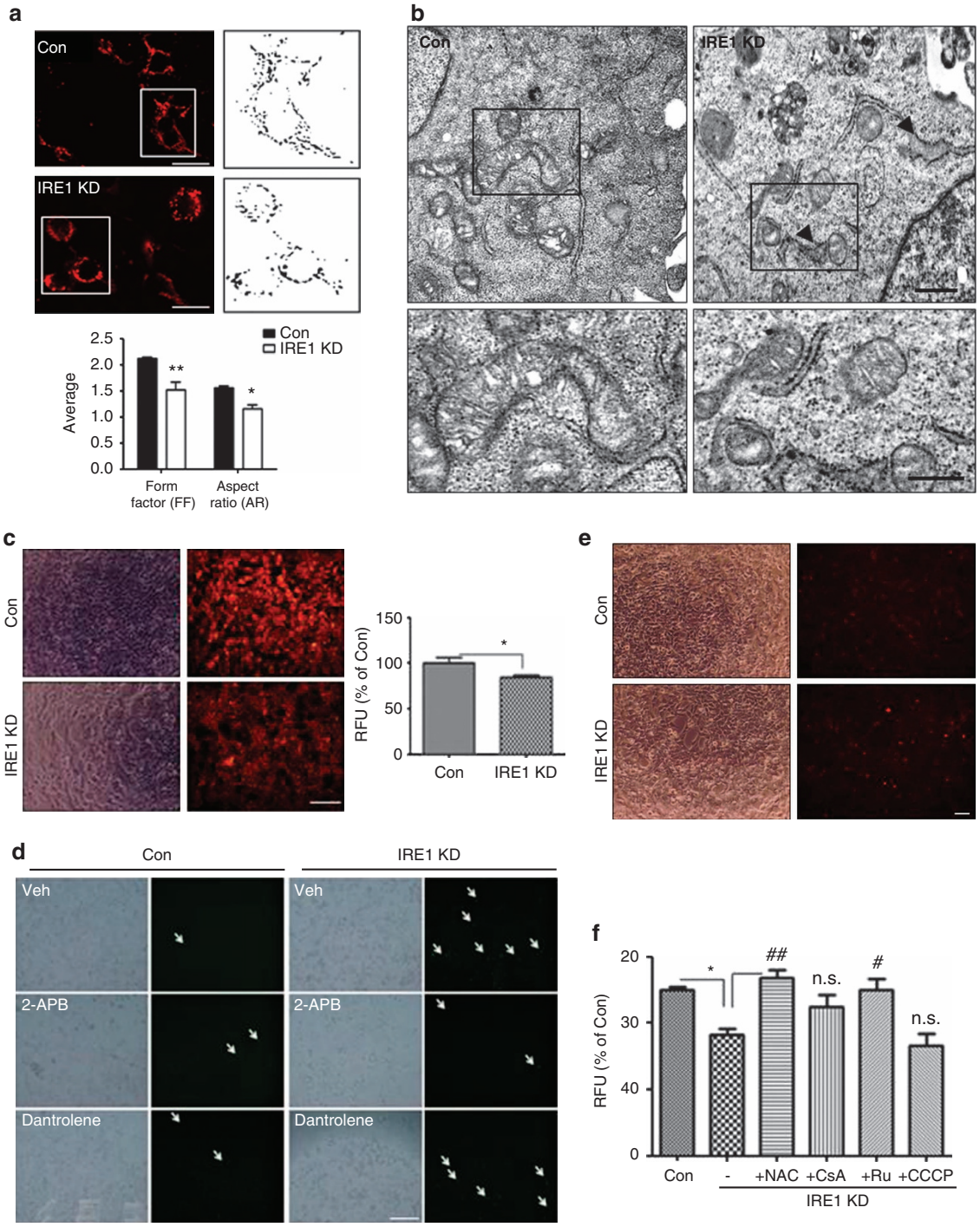

Figure 6 IRE1α KD induces mitochondrial dysfunction and ROS generation leading to cell death. (**a**) Changes in mitochondrial morphology in IRE1α-KD cells. Mitochondria in IRE1α-KD cells were shortened (represented by the aspect ratio) and had a more circular shape (represented by the form factor) in comparison with control siRNA-transfected cells. Scale bar = 20 μm. (**b**) EM images of IRE1α-KD cells showed mitochondrial fission. The lower panels show enlarged figures, and the arrowheads show expanded ER. Scale bar = 2 μm. (**c**) The mitochondrial membrane potential was measured by TMRM assay. Representative images are shown. Data presented are the mean ± S.E.M. of three experiments. $^{*}P<0.05$ *versus* control siRNA-transfected cells. Scale bar = 50 μm. (**d**) ROS generation in IRE1α-KD cells was determined by DCFDA staining. Arrow indicates DCF fluorescence (ROS generation). Treatment with InsP3R blocker (2-APB), not RyRs blocker (Dant; dantrolene), blocked the increase of ROS levels in the IRE1α-KD cells. After siRNA transfection for 36 h, dantrolene (20 μM) or 2-APB (10 μM) were added for 12 h. After washing, 1 μM DCFDA in OPTI-MEM was added at 37 °C for 60 min, and fluorescent signals were captured by fluorescence microscopy. Representative images are shown. ($N=3$ experiments); Scale bar = 50 μm. (**e**) Generation of mitochondrial superoxide in IRE1α-KD cells was measured by MitoSOX staining. Red fluorescence indicates the existence of mitochondrial superoxide. IRE1α-KD cells showed increased mitochondrial superoxide levels. Scale bar = 50 μm. (**f**) Treatment with ROS scavenger (NAC) or mitochondrial calcium uptake blocker (Ru360) blocked increased cell death in the IRE1α-KD cells. Cell viability was measured by calcein-AM assay. After siRNA transfection for 24 h, NAC (1 mM), CsA (200 nM), Ru360 (10 μM), and CCCP (2.5 μM) in DMEM were added for 24 h. After washing, the calcein-AM assay was performed. Data shown are the mean percentage ± S.E.M of four experiments. $^{*}P<0.01$ versus control siRNA-transfected cells; $^{\#}P<0.05$ $^{\#\#}P<0.01$ *versus* vehicle (DMSO)-treated IRE1α-KD cells. NS indicates no significant difference

mitochondrial membrane potential. The tetramethyl rhodamine methyl ester (TMRM) assay showed depolarization of mitochondrial membrane potential in IRE1α-KD cells (Figure 6c). Depolarized mitochondrial membrane potential induces ROS generation.[44] Dichlorofluorescein diacetate (DCFDA) staining showed increased DCF fluorescence, representing increased ROS levels in IRE1α-KD cells (Figure 6d). To detect mitochondrial superoxide accumulation, we performed MitoSOX Red staining and found that the IRE1α-KD cells showed significantly higher levels of MitoSOX Red fluorescence in mitochondria (Figure 6e). To determine whether alterations in mitochondrial homeostasis induce cell death under IRE1α-KD conditions, we performed the cell death assay with several blockers. Treatment with NAC, a well-known ROS scavenger, or Ru360, a blocker of the mitochondrial uniporter (MCU), rescued cell death caused by IRE1α KD (Figure 6f), indicating that IRE1α-KD-induced $[Ca^{2+}]_c$ increases enhanced Ca^{2+} load in the mitochondria, thereby leading to mitochondrial dysfunction and cell death. Notably, treatment with carbonyl cyanide m-chlorophenyl hydrazone (CCCP), the mitochondrial uncoupler, did not induce additional cell death in comparison with IRE1α KD alone (Figure 6f), suggesting that IRE1α KD induced cell death through mitochondrial dysfunction. Cyclosporin A (CsA), which inhibits mitochondrial permeability transition,[45] partially rescued the IRE1α-KD cells from cell death (Figure 6f). These results suggest that IRE1α KD induces mitochondrial dysfunction and cell death through increased ROS generation.

Discussion

Accumulating studies have shown that ER stress is closely associated with cell death.[21] As the ER mediates protein synthesis, folding, and Ca^{2+} maintenance, the ER disruption causes cell death through several mechanisms. In response to ER stress, the cells activate the ER stress-specific defense system.[3,4] It is well known that IRE1α acts as the main ER stress transducer;[6] however, its role in cell death is not yet fully understood. In this study, we chose SH-SY5Y cells based on previous reports on the roles of IRE1α in ER stress and mitochondria-ER crosstalk.[46,47] Our results demonstrate that cell death was induced in IRE1α knocked down SH-SY5Y cells (IRE1α-KD cells) compared with control siRNA-transfected cells (Con). As the ER is a Ca^{2+}-storing organelle, $[Ca^{2+}]_i$ increased when IRE1α was knocked down, and treatment with a Ca^{2+}-chelating agent rescued cell death induced by IRE1α KD. We explored the underlying mechanism of IRE1α-induced $[Ca^{2+}]_i$ increases and found that IRE1α-KD-induced $[Ca^{2+}]_i$ upregulation resulted from ER Ca^{2+} release. Our results also indicate that the ER Ca^{2+}-related channel InsP3R mediated IRE1α-KD-induced $[Ca^{2+}]_i$ increases, thereby leading to cell death. Previously, abnormal Ca^{2+} release from InsP3R has been suggested to

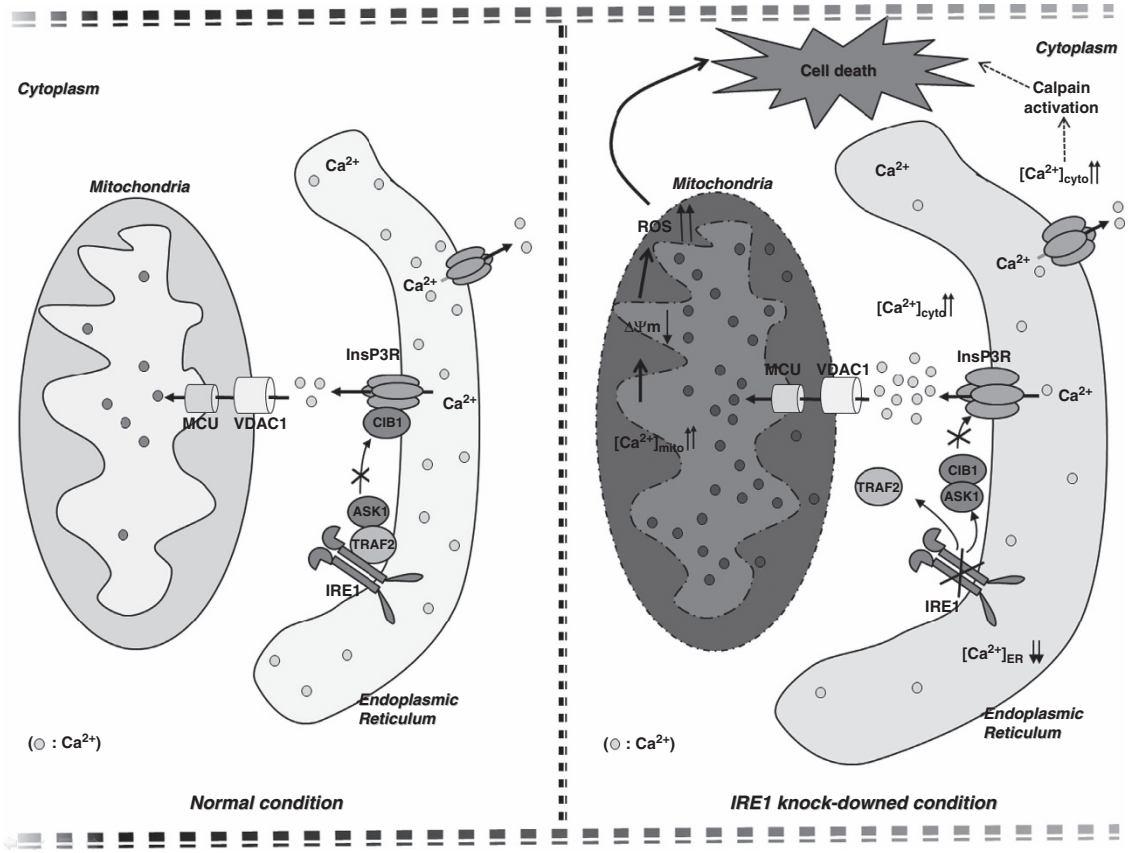

Figure 7 Proposed model of cell death in IRE1α-KD cells. Reduced IREα appeared to induce cell death through an accelerated ER-to-cytosolic efflux of calcium through InsP3R, followed by mitochondrial dysfunction and calpain-activated pathway

act as an important apoptotic signal.[48,49] Here, we found that treatment with InsP3R blockers inhibited $[Ca^{2+}]_i$ increases and cell death in the IRE1α-KD cells. In addition, treatment of SH-SY5Y cells with the InsP3R agonist adenophostin A caused significant cell death, whereas co-treatment with BAPTA-AM inhibited cell death (Supplementary Figures S4a and b). These results suggest that enhanced InsP3R-mediated Ca^{2+} release may induce cell death in a Ca^{2+}-dependent manner.

We explored the underlying mechanism of IRE1α-KD-induced InsP3R activation by co-IP and found that IRE1α did not interact with InsP3R directly. In previous studies of InsP3R's binding partners, CIB1 binding to InsP3R inhibited Ca^{2+} release from InsP3R,[22] and CIB1 is thought to function as a Ca^{2+}-sensitive modulator by interacting directly with ASK1.[41] We tested the association between opening of InsP3R and the CIB1-ASK1 interaction under IRE1α-KD conditions and found that IRE1α KD enhanced the CIB1-ASK1 interaction but reduced the CIB1-InsP3R interaction, which in turn resulted in increased Ca^{2+} release from InsP3R. There are previous studies that IRE1α-ASK1 pathway mediates cell death under pathological conditions.[8] In contrast, we focused on the role of IRE1α itself under normal condition. We compared with control siRNA-transfected cells and IRE1α siRNA-transfected cells without any stimuli. We found first that IRE1α regulates Ca^{2+} homeostasis in the ER by trapping ASK1. The downregulation of IRE1α induced the increased ASK1-CIB1 interaction through the decreased IRE1α-ASK1 interaction, resulting in the reduction of inhibitory roles of CIB1 in Ca^{2+} release through IP3R. Consistently, CIB1 KD increased $[Ca^{2+}]_i$, likely through reduced interaction between CIB1 and InsP3R and thus induced cell death (Figures 5d and e).

Mitochondria are the intracellular organelles associated with Ca^{2+} handling. Mitochondrial Ca^{2+} uptake regulates intracellular Ca^{2+} signaling and cell survival by buffering cytosolic Ca^{2+} levels.[50] Previous studies have shown that Ca^{2+} accumulation in mitochondria induced apoptotic cell death through Ca^{2+}-induced MPTP opening. As IRE1α KD induced $[Ca^{2+}]_i$ increases and cell death, we focused on mitochondrial alterations, including abnormal mitochondrial fission and reduced mitochondrial functions in the IRE1α-KD cells. In addition, IRE1α KD increased the levels of ROS, a well-known cell death-inducing factor. Ca^{2+} accumulation in mitochondria occurs via the MCU across a steep electrochemical gradient.[51] Treatment of IRE1α-KD cells with MCU blockers inhibited cell death, indicating that Ca^{2+} accumulation in mitochondria may act as a main apoptotic factor in the IRE1α-KD cells. We also found that ROS scavengers reduced cell death in the IRE1α-KD cells. Based on the finding that treatment of the IRE1α-KD cells with 2-APB reduced ROS generation (Figure 6d), we suggest that IRE1α-KD-induced $[Ca^{2+}]_{mito}$ accumulation caused increased ROS generation and eventually induced apoptotic cell death. Notably, IRE1α-KD-induced cell death was also mediated, at least in part, by calpain activation (Supplementary Figures S5a–d and Figure 7). Treatment of the IRE1α-KD cells with a calpain inhibitor blocked cell death induced by $[Ca^{2+}]_i$ upregulation. These results are consistent with previous studies showing that excessive Ca^{2+} binds and activates Ca^{2+}-dependent enzymes, such as calpain, thereby activating caspase-12 and triggering the apoptotic pathway.[52]

Surprisingly, unlike IRE1α, knockdown of the other two ER stress transducers, PERK and ATF6α, did not lead to $[Ca^{2+}]_i$ increases or cell death. In conclusion, reduced expression of the ER stress transducer IRE1α induced ER stress and caused cell death by accelerating ER Ca^{2+} release via InsP3R. InsP3R-induced ER Ca^{2+} release in the IRE1α-KD cells caused cell death via prolonged mitochondrial Ca^{2+} accumulation and alterations in ER morphology and function (Figure 7).

Materials and Methods

Cell cultures, transfection, and drug treatment. Human neuroblastoma SH-SY5Y cells were cultured in Dulbecco's modified Eagle's medium (DMEM; HyClone, Irvine, CA, USA) supplemented with 10% fetal bovine serum (HyClone) and an antibiotic mixture of penicillin (100 U/ml) and streptomycin (100 μg/ml). The control siRNA (sc-37007) and siRNA against IRE1α (sc-40705 and 1171247), PERK (1046373), ATF-6α (1009444), and CIB1 (sc-43271) were purchased from Santa Cruz Biotechnology (Santa Cruz, CA, USA) and/or Bioneer Inc. (Daejeon, Korea). Cy3-tagged IRE1α siRNA was made by Bioneer, Inc. and IRE1α cDNA was purchased from Addgene (ID:20744; Cambridge, MA, USA). Cells were cultured for 48 h after transfection with Lipofectamine for cDNA and RNAimax for siRNA according to the manufacturer's instructions (Invitrogen, Carlsbad, CA, USA) and treated with vehicle or appropriate concentrations of TUDCA (T0266), tunicamycin (T7765), thapsigargin (T9033), BAPTA-AM (A1076), CCCP (C2759), dantrolene (D9175), 2-APB (D9754), *N*-acetyl-L-cysteine (NAC) (A7250), L-NG-nitroarginine methyl ester (N5751), CsA (30024), and Calpain Inhibitor I (A6185) from Sigma-Aldrich (St. Louis, MO, USA); Xestospongin C (sc-201505) and Ru360 (sc-222265) from Santa Cruz Biotechnology; DEVD-fmk (550378) from BD Biosciences (Franklin Lakes, NJ, USA); 1-tert-butyl-3-naphthalen-1-ylmethyl-1 H-pyrazolo[3,4–d]pyrimidin-4-ylamine (1NM-PP1) (13330) from Cayman Chemical (Ann Arbor, MI, USA); and adenophostin A (115500) from Calbiochem (San Diego, CA, USA). Sequences were as follows: siRNA against IRE1α (1171247) 5′-CUGCUUAAUGUCAGUCUAC-3′ (sense), 5′-GUAGACUGA CAUUAAGCAG-3′ (antisense); siRNA against PERK (1046373) 5′-GAGAACACA GAAGAGUCUA-3′ (sense), 5′-UAGACUCUUCUGUGUUCUC-3′ (antisense); and siRNA against ATF-6α (1009444) 5′-CAGAGAACUGUCUCGUACU-3′ (sense), 5′-AGUACGAGACAGUUCUCUG-3′ (antisense).

Antibodies. Cell pellets were prepared as described[53] and western blotted with the following antibodies: anti-IRE1α (ab37073; 1 : 1500) from Abcam (Cambridge, MA, USA); anti-β-actin (A1978; 1 : 5000) from Sigma-Aldrich; anti-PERK (sc-13073; 1 : 1000), anti-ATF6α (sc-22799; 1 : 1000), anti-GADD153 (sc-575; 1 : 1000), anti-ASK1 (sc-7931 and sc-5294; 1 : 1000 for WB, 1 : 100 for IP and PLA), anti-caspase-12 (sc-70227; 1 : 1000), anti-GRP78 (sc-1050; 1 : 1000), anti-TRAF2 (sc-7346; 1 : 1000), and anti-calpain (sc-7530; 1 : 1000) (Santa Cruz Biotechnology); anti-ryanodine receptor (MA3-916; 1 : 1000) (Thermo Scientific, Hudson, NH, USA); anti-InsP3R (07-1210; 1 : 2000 for WB, 1 : 300 for IP, 1 : 100 for PLA) and anti-CIB1 (MAB2601; 1 : 1500 for WB, 1 : 500 for IP, 1 : 100 for PLA) (Millipore, Schwalbach, Germany); and anti-calreticulin (2891; 1 : 2000), anti-calnexin (2433; 1 : 2000), anti-cleaved caspase-9 (9501; 1 : 2000), anti-caspase-9 (9502; 1 : 2000), and anti-caspase-3 (9662; 1 : 2000) (Cell Signaling Technology, Beverly, MA, USA). Immunoreactive bands were photographed and quantified on LAS-3000 with MultiGauge (Fuji Film Inc., Tokyo, Japan).

Live and dead cell assay. To measure cell viability, calcein-AM, MTT, and TUNEL assays were performed.[54] The calcein-AM assay was performed according to the manufacturer's instructions (C3099, LIVE/DEAD Viability and Cytotoxicity Kit; Molecular Probes, Invitrogen, Carlsbad, CA, USA). Briefly, 5×10^3 cells were incubated for 24 h after seeding in 96-well plate, and then transfected with 20–50 pM siRNA for 24–48 h. Treatments were administered after transfection at optimal dose (see figure legends). Calcein-AM reagent in phenol red-free media (1 μM) was added, incubated for 1 h at 37 °C, and washed three times with PBS. Fluorescence was measured at excitation and emission wavelengths (ex/em) of 485 nm/530 nm on a fluorescence plate reader (Infinite M200 Pro; TECAN, Männendorf, Switzerland). The MTT assay was performed as described,[54] Briefly, after transfection and drug treatment, 2.5 mg/ml MTT (M2003; Sigma-Aldrich) in phenol red-free medium was

added and incubated for 2 h at 37 °C, followed by aspiration of the MTT solution, addition of isopropanol to dissolve the formazan crystals, and incubation at 37 °C for 1 h. Absorbance was measured at 540 nm. Experiments were independently repeated at least three times, and data were expressed as a percentage of the control (control siRNA-transfected or vehicle-treated cells). The TUNEL assay (G7361; Promega, Madison, WI, USA) was performed according to the manufacturer's protocol. Cells (1×10^3) were incubated for 24 h after seeding in 96-well plates and transfected with control or IRE1α siRNA for 48 h. TUNEL-positive cells were counted under a fluorescence microscope (Olympus, Tokyo, Japan) and expressed as the percentage of apoptotic cells relative to counted cells ($n = 500$) in 96 wells.

ROS measurement. Hydrogen peroxide levels were determined using DCFDA (C6827; Invitrogen). In brief, treated cells were incubated with 1 μM DCFDA for 30 min and washed with PBS. Fluorescent signals were captured using a fluorescence microscope. Changes in mitochondrial oxidant production were measured using MitoSOX Red staining (5 mM for 15 min at 37 °C; M36008; Invitrogen), according to the manufacturer's instructions.

Mitochondrial membrane potential measurement. In depolarized cells, mitochondrial labeling with potential-indicating probes like TMRM disappears; therefore, red fluorescence serves as an indicator of mitochondrial membrane potential. The medium was replaced with phenol red-free medium containing 500 nM TMRM (100 μl/well; T-668; Invitrogen). Plates were incubated for 1 h at 37 °C and washed three times with PBS (50 μl/well). Fluorescent signals were captured using a fluorescence microscope (Olympus), and analyzed in > 500 cells per group.

Morphology of mitochondria. Mitochondria were visualized after the expression of Mito-DsRed (DsRed2 fused to the mitochondrial targeting sequence from subunit VIII of human cytochrome *c* oxidase).[55] Images were captured under a confocal laser scanning microscope (FV10i-w; Olympus), and analyzed in 100 cells per group with the ImageJ software (National Institutes of Health, Bethesda, MD, USA).

Fluo-4 fluorescence imaging for $[Ca^{2+}]_i$ measurement. For intracellular Ca^{2+} imaging, cells were loaded with the Ca^{2+}-sensitive dye fluo-4-acetoxymethyl ester (Fluo-4 AM, 5 μM; F10471; Invitrogen) at 37 °C for 60 min and washed with PBS to remove extracellular Fluo-4 AM. After drug treatment, fluorescent signals were captured using a fluorescence microscope. The fluorescence intensity reflected $[Ca^{2+}]_i$. Images for 1000 cells per group were analyzed with the ImageJ software.

Fura-2 intracellular calcium imaging. Cytosolic calcium levels ($[Ca^{2+}]_c$) were assessed by ratiometric analysis using fura-2 acetoxymethyl ester (Fura-2 AM; F1221; Molecular Probes). Fura-2 AM was applied in the perfusion system throughout the imaging process. SH-SY5Y cells plated on poly-D-lysine-coated coverslips were loaded with Fura-2 AM (2 μM) for 30 min in Normal Tyrode's solution (140 mM NaCl, 5 mM KCl, 2 mM $CaCl_2$, 1 mM $MgCl_2$, 10 mM glucose, and 10 mM HEPES, pH 7.35), supplemented with 0.01% pluronic acid. Imaging was performed using an inverted microscope (Nikon Ti, Tokyo, Japan) with a × 40 UV objective lens (Nikon, Tokyo, Japan). Fura-2 AM was excited by sequential illuminations at 340 and 380 nm from a Lambda DG-4 illumination system (Sutter, Novato, CA, USA). Image processing was controlled by the Axon Imaging Workbench software 6.0 (AIW; Union City, CA, USA). Emission was detected at a wavelength of 510 nm. Fura-2 emission ratios following excitation at 340 and 380 nm were processed by AIW. Video images were obtained using an intensified CCD camera (LUCA; Andor, Belfast, UK). The analysis and plotting were carried out in the Origen 8.0 software (OriginLab Corp., Northampton, MA, USA).

Immunocytochemistry. Immunocytochemical staining was performed as described.[56] Briefly, cells were fixed for 15 min in 4% paraformaldehyde/PBS. After blocking, the cells were incubated with primary antibodies overnight at 4 °C. After washing with PBS, the cells were incubated for 1 h at room temperature with fluorescent-labeled secondary antibodies (1 : 500; Invitrogen). Cells were counter-stained with DAPI for 10 min. Images were captured with a confocal laser-scanning microscope (FV10i-w).

Proximity ligation assay (PLA). Cells fixed with cold acetone were analyzed using the Duolink Kit (Olink Bioscience, Uppsala, Sweden) according to the manufacturer's instructions. Briefly, samples were incubated with anti-ASK1 (rabbit polyclonal), anti-CIB1 (mouse monoclonal), and anti-InsP3R (rabbit polyclonal) antibodies, followed by addition of secondary antibodies conjugated with oligonucleotides (PLA probe MINUS and PLA probe PLUS). Oligonucleotides in hybridization solution will hybridize to two PLA probes if they are in close proximity (< 40 nm). A ligase (Ligation Solution), nucleotides, and polymerase were added sequentially, allowing the formation of rolling-circle amplification products, which can be detected via labeled oligonucleotides. Signals visible as distinct dots were analyzed by confocal laser microscopy (FV10i-w).

Co-IP. For immunoprecipitation (IP), cell pellets were resuspended in IP buffer (150 mM Tris-HCl, pH 6.8, 10 mM EDTA, 0.25% CHAPS) containing protease inhibitors (Sigma-Aldrich), followed by centrifugation at 13 000 r.p.m. for 15 min. To eliminate non-specific binding, a preclearing step was performed with protein A/G agarose beads (Santa Cruz) for 1 h. Next, samples were centrifuged for 5 min at 2000 × *g*. Equal amounts of protein were precipitated with specific antibodies at 4 °C overnight on a rocker. Protein A/G agarose beads were added to each sample and incubated at 4 °C for 2 h. Immunoprecipitates were collected by centrifugation and washed three times with the same buffer. Finally, agarose beads were resuspended in 50 μl of 1 × SDS-PAGE sample buffer and incubated at 55 °C for 10 min to release the proteins. After a pulse spin, supernatants were analyzed by SDS-PAGE.

EM. SH-SY5Y cells were fixed overnight in a mixture of cold 2.5% glutaraldehyde in 0.1 M phosphate buffer (pH 7.2) and 2% paraformaldehyde in 0.1 M phosphate or cacodylate buffer (pH 7.2) and then embedded with epoxy resin. Epoxy resin-mixed samples were loaded into capsules and allowed to polymerize at 38 °C for 12 h and 60 °C for 48 h. Thin sections were sliced on an ultramicrotome (RMC MT-XL) and collected on a copper grid. Appropriate areas for thin sectioning were cut at 65 nm and stained with saturated 4% uranyl acetate and 4% lead citrate, followed by examination under a transmission electron microscope (JEM-1400; Tokyo, Japan) at 80 kV.

Data analysis. For western blots, protein levels were normalized to pan forms or a housekeeping protein, such as β-actin. All data were expressed as means ± S.E.M. Student's *t*-test was used for two-group comparisons, and analysis of variance, followed by Fisher's LSD *post hoc* test to compare three or more groups using SigmaStat for Windows Version 3.10 (Systat Software, Inc., Point Richmond, CA, USA). *P* values of < 0.05 were considered statistically significant.

Conflict of Interest

The authors declare no conflict of interest.

Acknowledgements. This work was supported by grants from the NRF (2012R1A2A1A01002881, MRC (2011–0030738)), the KNIH ROAD R&D Program Project (A092058 to IM-J), and KRIBB Research Initiative Program.

Author contributions

SMS wrote the manuscript and researched data. JB researched data. S-ER, SJK researched Ca^{2+} data. IM-J supervised the study and reviewed and edited the manuscript.

1. Meldolesi J, Pozzan T. The endoplasmic reticulum Ca2 + store: a view from the lumen. *Trends Biochem Sci* 1998; **23**: 10–14.
2. Ma Y, Hendershot LM. The unfolding tale of the unfolded protein response. *Cell* 2001; **107**: 827–830.
3. Kaufman RJ. Orchestrating the unfolded protein response in health and disease. *J Clin Invest* 2002; **110**: 1389–1398.
4. Ron D, Walter P. Signal integration in the endoplasmic reticulum unfolded protein response. *Nat Rev Mol Cell Biol* 2007; **8**: 519–529.
5. Schroder M, Kaufman RJ. The mammalian unfolded protein response. *Annu Rev Biochem* 2005; **74**: 739–789.
6. Shamu CE, Walter P. Oligomerization and phosphorylation of the Ire1p kinase during intracellular signaling from the endoplasmic reticulum to the nucleus. *EMBO J* 1996; **15**: 3028–3039.
7. Yoshida H, Matsui T, Yamamoto A, Okada T, Mori K. XBP1 mRNA is induced by ATF6 and spliced by IRE1 in response to ER stress to produce a highly active transcription factor. *Cell* 2001; **107**: 881–891.

8. Urano F, Wang X, Bertolotti A, Zhang Y, Chung P, Harding HP *et al.* Coupling of stress in the ER to activation of JNK protein kinases by transmembrane protein kinase IRE1. *Science* 2000; **287**: 664–666.
9. Nishitoh H, Matsuzawa A, Tobiume K, Saegusa K, Takeda K, Inoue K *et al.* ASK1 is essential for endoplasmic reticulum stress-induced neuronal cell death triggered by expanded polyglutamine repeats. *Genes Dev* 2002; **16**: 1345–1355.
10. Harding HP, Zhang Y, Ron D. Protein translation and folding are coupled by an endoplasmic-reticulum-resident kinase. *Nature* 1999; **397**: 271–274.
11. Rutkowski DT, Kaufman RJ. All roads lead to ATF4. *Dev Cell* 2003; **4**: 442–444.
12. Ye J, Rawson RB, Komuro R, Chen X, Dave UP, Prywes R *et al.* ER stress induces cleavage of membrane-bound ATF6 by the same proteases that process SREBPs. *Mol Cell* 2000; **6**: 1355–1364.
13. Carafoli E. Calcium signaling: a tale for all seasons. *Proc Natl Acad Sci USA* 2002; **99**: 1115–1122.
14. Gorlach A, Klappa P, Kietzmann T. The endoplasmic reticulum: folding, calcium homeostasis, signaling, and redox control. *Antioxid Redox Signal* 2006; **8**: 1391–1418.
15. Bezprozvanny I. The inositol 1,4,5-trisphosphate receptors. *Cell Calcium* 2005; **38**: 261–272.
16. Rossi D, Sorrentino V. Molecular genetics of ryanodine receptors Ca2 + -release channels. *Cell Calcium* 2002; **32**: 307–319.
17. East JM. Sarco(endo)plasmic reticulum calcium pumps: recent advances in our understanding of structure/function and biology (review). *Mol Membr Biol* 2000; **17**: 189–200.
18. Squier MK, Sehnert AJ, Sellins KS, Malkinson AM, Takano E, Cohen JJ. Calpain and calpastatin regulate neutrophil apoptosis. *J Cell Physiol* 1999; **178**: 311–319.
19. Wang HG, Pathan N, Ethell IM, Krajewski S, Yamaguchi Y, Shibasaki F *et al.* Ca2 + -induced apoptosis through calcineurin dephosphorylation of BAD. *Science* 1999; **284**: 339–343.
20. Nakagawa T, Zhu H, Morishima N, Li E, Xu J, Yankner BA *et al.* Caspase-12 mediates endoplasmic-reticulum-specific apoptosis and cytotoxicity by amyloid-beta. *Nature* 2000; **403**: 98–103.
21. Kim I, Xu W, Reed JC. Cell death and endoplasmic reticulum stress: disease relevance and therapeutic opportunities. *Nat Rev Drug Discov* 2008; **7**: 1013–1030.
22. Hennigs JK, Burhenne N, Stahler F, Winnig M, Walter B, Meyerhof W *et al.* Sweet taste receptor interacting protein CIB1 is a general inhibitor of InsP3-dependent Ca2 + release in vivo. *J Neurochem* 2008; **106**: 2249–2262.
23. Rao RV, Hermel E, Castro-Obregon S, del Rio G, Ellerby LM, Ellerby HM *et al.* Coupling endoplasmic reticulum stress to the cell death program. Mechanism of caspase activation. *J Biol Chem* 2001; **276**: 33869–33874.
24. Tirasophon W, Welihinda AA, Kaufman RJ. A stress response pathway from the endoplasmic reticulum to the nucleus requires a novel bifunctional protein kinase/endoribonuclease (Ire1p) in mammalian cells. *Genes Dev* 1998; **12**: 1812–1824.
25. Oyadomari S, Mori M. Roles of CHOP/GADD153 in endoplasmic reticulum stress. *Cell Death Differ* 2004; **11**: 381–389.
26. Cox JS, Shamu CE, Walter P. Transcriptional induction of genes encoding endoplasmic reticulum resident proteins requires a transmembrane protein kinase. *Cell* 1993; **73**: 1197–1206.
27. Bommiasamy H, Back SH, Fagone P, Lee K, Meshinchi S, Vink E *et al.* ATF6alpha induces XBP1-independent expansion of the endoplasmic reticulum. *J Cell Sci* 2009; **122**(Pt 10): 1626–1636.
28. Pineau L, Colas J, Dupont S, Beney L, Fleurat-Lessard P, Berjeaud JM *et al.* Lipid-induced ER stress: synergistic effects of sterols and saturated fatty acids. *Traffic* 2009; **10**: 673–690.
29. Xie Q, Khaoustov VI, Chung CC, Sohn J, Krishnan B, Lewis DE *et al.* Effect of tauroursodeoxycholic acid on endoplasmic reticulum stress-induced caspase-12 activation. *Hepatology* 2002; **36**: 592–601.
30. Reimertz C, Kogel D, Rami A, Chittenden T, Prehn JH. Gene expression during ER stress-induced apoptosis in neurons: induction of the BH3-only protein Bbc3/PUMA and activation of the mitochondrial apoptosis pathway. *J Cell Biol* 2003; **162**: 587–597.
31. Thastrup O. Role of Ca2(+)-ATPases in regulation of cellular Ca2 + signalling, as studied with the selective microsomal Ca2(+)-ATPase inhibitor, thapsigargin. *Agents Actions* 1990; **29**: 8–15.
32. Berridge MJ. The endoplasmic reticulum: a multifunctional signaling organelle. *Cell Calcium* 2002; **32**: 235–249.
33. Supattapone S, Worley PF, Baraban JM, Snyder SH. Solubilization, purification, and characterization of an inositol trisphosphate receptor. *J Biol Chem* 1988; **263**: 1530–1534.
34. Ellisman MH, Deerinck TJ, Ouyang Y, Beck CF, Tanksley SJ, Walton PD *et al.* Identification and localization of ryanodine binding proteins in the avian central nervous system. *Neuron* 1990; **5**: 135–146.
35. Gunteski-Hamblin AM, Greeb J, Shull GE. A novel Ca2 + pump expressed in brain, kidney, and stomach is encoded by an alternative transcript of the slow-twitch muscle sarcoplasmic reticulum Ca-ATPase gene. Identification of cDNAs encoding Ca2 + and other cation-transporting ATPases using an oligonucleotide probe derived from the ATP-binding site. *J Biol Chem* 1988; **263**: 15032–15040.
36. Slee EA, Harte MT, Kluck RM, Wolf BB, Casiano CA, Newmeyer DD *et al.* Ordering the cytochrome c-initiated caspase cascade: hierarchical activation of caspases-2, -3, -6, -7, -8, and -10 in a caspase-9-dependent manner. *J Cell Biol* 1999; **144**: 281–292.
37. Thornberry NA, Lazebnik Y. Caspases: enemies within. *Science* 1998; **281**: 1312–1316.
38. Sadowski-Debbing K, Coy JF, Mier W, Hug H, Los M. Caspases—their role in apoptosis and other physiological processes as revealed by knock-out studies. *Arch Immunol Ther Exp (Warsz)* 2002; **50**: 19–34.
39. Gafni J, Munsch JA, Lam TH, Catlin MC, Costa LG, Molinski TF *et al.* Xestospongins: potent membrane permeable blockers of the inositol 1,4,5-trisphosphate receptor. *Neuron* 1997; **19**: 723–733.
40. Han D, Upton JP, Hagen A, Callahan J, Oakes SA, Papa FR. A kinase inhibitor activates the IRE1alpha RNase to confer cytoprotection against ER stress. *Biochem Biophys Res Commun* 2008; **365**: 777–783.
41. Yoon KW, Cho JH, Lee JK, Kang YH, Chae JS, Kim YM *et al.* CIB1 functions as a Ca(2 +)-sensitive modulator of stress-induced signaling by targeting ASK1. *Proc Natl Acad Sci USA* 2009; **106**: 17389–17394.
42. Szalai G, Krishnamurthy R, Hajnoczky G. Apoptosis driven by IP(3)-linked mitochondrial calcium signals. *EMBO J* 1999; **18**: 6349–6361.
43. Hajnoczky G, Csordas G, Das S, Garcia-Perez C, Saotome M, Sinha Roy S *et al.* Mitochondrial calcium signalling and cell death: approaches for assessing the role of mitochondrial Ca2 + uptake in apoptosis. *Cell Calcium* 2006; **40**: 553–560.
44. Lee I, Bender E, Kadenbach B. Control of mitochondrial membrane potential and ROS formation by reversible phosphorylation of cytochrome c oxidase. *Mol Cell Biochem* 2002; **234-235**: 63–70.
45. Hansson MJ, Mansson R, Mattiasson G, Ohlsson J, Karlsson J, Keep MF *et al.* Brain-derived respiring mitochondria exhibit homogeneous, complete and cyclosporin-sensitive permeability transition. *J Neurochem* 2004; **89**: 715–729.
46. Lee H, Noh JY, Oh Y, Kim Y, Chang JW, Chung CW *et al.* IRE1 plays an essential role in ER stress-mediated aggregation of mutant huntingtin via the inhibition of autophagy flux. *Hum Mol Genet* 2012; **21**: 101–114.
47. De Simoni S, Linard D, Hermans E, Knoops B, Goemaere J. Mitochondrial peroxiredoxin-5 as potential modulator of mitochondria-ER crosstalk in MPP(+) -induced cell death. *J Neurochem* 2012; **125**: 473–485.
48. Jayaraman T, Marks AR. T cells deficient in inositol 1,4,5-trisphosphate receptor are resistant to apoptosis. *Mol Cell Biol* 1997; **17**: 3005–3012.
49. Jayaraman T, Marks AR. Calcineurin is downstream of the inositol 1,4,5-trisphosphate receptor in the apoptotic and cell growth pathways. *J Biol Chem* 2000; **275**: 6417–6420.
50. Rizzuto R, De Stefani D, Raffaello A, Mammucari C. Mitochondria as sensors and regulators of calcium signalling. *Nat Rev Mol Cell Biol* 2012; **13**: 566–578.
51. Kirichok Y, Krapivinsky G, Clapham DE. The mitochondrial calcium uniporter is a highly selective ion channel. *Nature* 2004; **427**: 360–364.
52. He P, Wang AG, Xia T, Gao P, Niu Q, Guo LJ *et al.* Mechanism of the neurotoxic effect of PBDE-47 and interaction of PBDE-47 and PCB153 in enhancing toxicity in SH-SY5Y cells. *Neurotoxicology* 2009; **30**: 10–15.
53. Son SM, Jung ES, Shin HJ, Byun J, Mook-Jung I. Abeta-induced formation of autophagosomes is mediated by RAGE-CaMKKbeta-AMPK signaling. *Neurobiol Aging* 2012; **33**: 1006 e1011–1006 e1023.
54. Cha MY, Han SH, Son SM, Hong HS, Choi YJ, Byun J *et al.* Mitochondria-specific accumulation of amyloid beta induces mitochondrial dysfunction leading to apoptotic cell death. *PLoS One* 2012; **7**: e34929.
55. Rizzuto R, Brini M, Pizzo P, Murgia M, Pozzan T. Chimeric green fluorescent protein as a tool for visualizing subcellular organelles in living cells. *Curr Biol* 1995; **5**: 635–642.
56. Son SM, Song H, Byun J, Park KS, Jang HC, Park YJ *et al.* Altered APP processing in insulin-resistant conditions is mediated by autophagosome accumulation via the inhibition of mammalian target of rapamycin pathway. *Diabetes* 2012; **61**: 3126–3138.

Supplementary Information accompanies this paper on Cell Death and Disease website (http://www.nature.com/cddis)